



LUND UNIVERSITY

High-precision Mass Measurements of 203-207Rn and 213Ra with SHIPTRAP

Droese, C.; Ackermann, D.; Andersson, L. -L.; Blaum, K.; Block, M.; Dworschak, M.; Eibach, M.; Eliseev, S.; Forsberg, Ulrika; Haettner, E.; Herfurth, F.; Hessberger, F. P.; Hofmann, S.; Ketelaer, J.; Marx, G.; Ramirez, E. Minaya; Nesterenko, D.; Novikov, Yu. N.; Plass, W. R.; Rodriguez, D.; Rudolph, Dirk; Scheidenberger, C.; Schweikhard, L.; Stolze, S.; Thierolf, P. G.; Weber, C.

Published in:

European Physical Journal A. Hadrons and Nuclei

DOI:

[10.1140/epja/i2013-13013-0](https://doi.org/10.1140/epja/i2013-13013-0)

2013

[Link to publication](#)

Citation for published version (APA):

Droese, C., Ackermann, D., Andersson, L. -L., Blaum, K., Block, M., Dworschak, M., Eibach, M., Eliseev, S., Forsberg, U., Haettner, E., Herfurth, F., Hessberger, F. P., Hofmann, S., Ketelaer, J., Marx, G., Ramirez, E. M., Nesterenko, D., Novikov, Y. N., Plass, W. R., ... Weber, C. (2013). High-precision Mass Measurements of 203-207Rn and 213Ra with SHIPTRAP. *European Physical Journal A. Hadrons and Nuclei*, 49(1), 13-19. <https://doi.org/10.1140/epja/i2013-13013-0>

Total number of authors:

26

General rights

Unless other specific re-use rights are stated the following general rights apply:

Copyright and moral rights for the publications made accessible in the public portal are retained by the authors and/or other copyright owners and it is a condition of accessing publications that users recognise and abide by the legal requirements associated with these rights.

- Users may download and print one copy of any publication from the public portal for the purpose of private study or research.
- You may not further distribute the material or use it for any profit-making activity or commercial gain
- You may freely distribute the URL identifying the publication in the public portal

Read more about Creative commons licenses: <https://creativecommons.org/licenses/>

Take down policy

If you believe that this document breaches copyright please contact us providing details, and we will remove access to the work immediately and investigate your claim.

LUND UNIVERSITY

PO Box 117
221 00 Lund
+46 46-222 00 00

High-precision mass measurements of $^{203-207}\text{Rn}$ and ^{213}Ra with SHIPTRAP

C. Droese¹, D. Ackermann², L.-L. Andersson^{3,4}, K. Blaum^{5,6}, M. Block², M. Dworschak², M. Eibach^{5,7}, S. Eliseev⁵, U. Forsberg⁸, E. Haettner^{2,9}, F. Herfurth², F.P. Heßberger^{2,4}, S. Hofmann², J. Ketelaer⁵, G. Marx¹, E. Minaya Ramirez⁴, D. Nesterenko¹⁰, Yu. N. Novikov¹⁰, W. R. Plaß^{2,9}, D. Rodríguez¹¹, D. Rudolph⁸, C. Scheidenberger^{2,9}, L. Schweikhard¹, S. Stolze¹², P.G. Thirolf¹³, and C. Weber¹³

¹ Ernst-Moritz-Arndt-Universität, Felix-Hausdorff-Straße 6, 17489 Greifswald, Germany

² GSI Helmholtzzentrum für Schwerionenforschung, Planckstraße 1, 64291 Darmstadt, Germany

³ University of Liverpool, Liverpool L69 7ZE, United Kingdom

⁴ Helmholtz-Institut Mainz, Johannes Gutenberg-Universität, Johann-Joachim-Becher-Weg 36, 55099 Mainz, Germany

⁵ Max-Planck-Institut für Kernphysik, Saupfercheckweg 1, 69117 Heidelberg, Germany

⁶ Ruprecht-Karls-Universität Heidelberg, Albert-Ueberle-Str. 3-5, 69120 Heidelberg, Germany

⁷ Johannes Gutenberg-Universität Mainz, Saarstr. 21, 55122 Mainz, Germany

⁸ Lund University, Sölvegatan 37, 22362 Lund, Sweden

⁹ Justus-Liebig-Universität Gießen, Heinrich-Buff-Ring 14-16, 35392 Gießen, Germany

¹⁰ PNPI, NRC Kurchatov Institute, Gatchina, 188300 St. Petersburg, Russia

¹¹ Universidad de Granada, Campus de Fuentenueva, 18071 Granada, Spain

¹² University of Jyväskylä, Seminaarinkatu 15, 40014 Jyväskylä, Finland

¹³ Ludwig Maximilians-Universität München, Am Coulombwall 1, 85748 Garching, Germany

Received: 20.06.12 / Revised version: 18.09.12

Abstract. The masses of the nuclides $^{203-207}\text{Rn}$ and ^{213}Ra were measured directly for the first time with the Penning-trap mass spectrometer SHIPTRAP at GSI Darmstadt. The results confirm the previously determined mass values. The mass uncertainties for ^{205}Rn and ^{213}Ra were significantly reduced. The results are relevant for the investigation of the nuclear shell structure between $N = 82$ and $N = 126$. As an indicator of structural changes the two-neutron separation energies $S_{2n}(Z, N)$ have been studied.

1 Introduction

Nuclear masses give access to nuclear binding energies. High-precision mass measurements thus provide valuable information on pressing questions in nuclear physics, *e.g.* the formation of halo nuclei [1], the generation of heavy elements in the universe [2, 3] or the nuclear structure of superheavy elements [4, 5]. Penning traps are state-of-the-art tools to directly measure atomic masses with relative uncertainties of typically 10^{-8} [6, 7]. From such accurate mass values several characteristic indicators of nuclear structure effects like the two-neutron separation energy $S_{2n}(Z, N)$ can be derived.

Here, we investigate the shell-structure evolution along the Rn isotopic chain between $N = 117$ and $N = 121$.

In the following, we report on the masses of the neutron-deficient $^{203-207}\text{Rn}$ ($N = 117 - 121$) and ^{213}Ra ($N = 125$), which were measured directly for the first time (see Fig. 1). Their mass values listed in the Atomic-Mass Evaluation 2003 were determined via alpha-decay energies and the masses of their daughter nuclides that were directly measured by the ESR storage ring at GSI [8]. The properties of the investigated nuclei are of interest due to their vicinity to the closed proton shell at $Z=82$. Furthermore, these nuclei are connected via alpha-

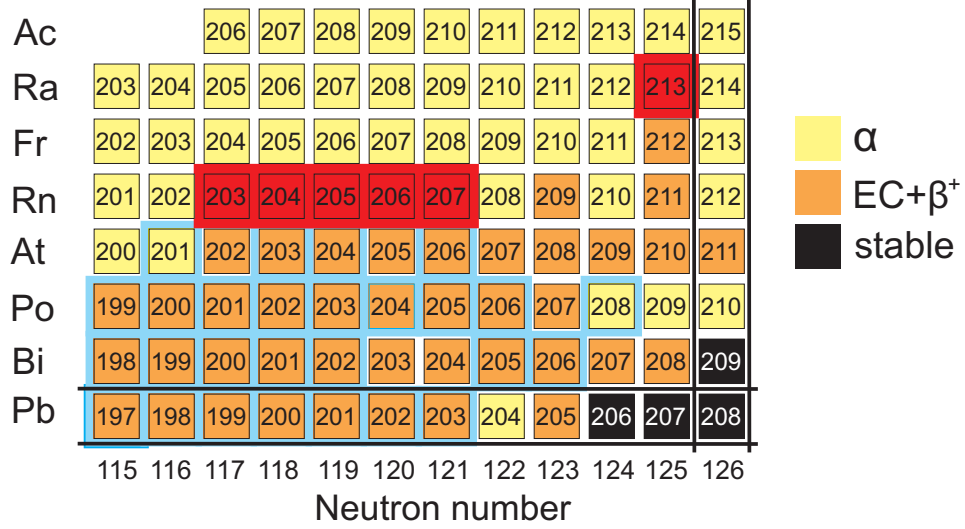


Fig. 1: (color online) Excerpt of the nuclide chart illustrating the nuclides discussed in this work highlighted in red. In addition, the dominant decay mode for each nuclide, a fraction of the nuclides investigated by the ESR [8] (blue frame) and the closed proton and neutron shells (black lines) are shown.

decay chains to nuclei up to uranium and, therefore, their precise mass determination helps to improve the mass values of heavier elements. While in the case of ^{203}Rn the mass of the long-lived excited state was measured, for all other nuclides the ground-state mass has been determined. Some of the relevant nuclear properties of the ground states and the known isomeric states of the investigated nuclides are presented in Table 1. The results are compared to previously published values and nuclear shell effects are discussed using the obtained S_{2n} values.

2 Experimental setup and methods

The investigations were performed with the Penning-trap mass spectrometer SHIPTRAP [4, 9] at GSI/Darmstadt. SHIPTRAP (see Fig. 2) is installed behind the velocity filter SHIP (Separator for Heavy Ion reaction Products) [10].

In this work, the results of three measurement periods are discussed: In the first experiment in August 2009, ^{48}Ca projectiles were accelerated to an energy of 4.4 MeV/u with the UNILAC and reacted with a dysprosium target ($470\text{ }\mu\text{g}/\text{cm}^2$ with natural isotope abundances) to produce $^{204-207}\text{Rn}$. In addition, an erbium target

Table 1: Nuclear properties [11, 12] of the investigated nuclei. The first column gives the nuclide. The second column is the excitation energy of known isomeric states E_{level} followed by the half-life $T_{1/2}$ and the spin and parity J^π . The spin parity values in brackets indicate tentative assignments.

Nuclide	E_{level} / keV	$T_{1/2}$ / s	J^π
^{203}Rn	0	44(2)	(3/2 ⁻)
^{203m}Rn	362(5)	26.9(5)	(13/2 ⁺)
^{204}Rn	0	74.5(14)	0 ⁺
^{205}Rn	0	170(4)	5/2 ⁻
^{205m}Rn	657.1(5)	> 10	(13/2 ⁺)
^{206}Rn	0	340(10)	0 ⁺
^{207}Rn	0	555(10)	5/2 ⁻
^{207m}Rn	899.1(10)	$184.5(9) \cdot 10^{-6}$	13/2 ⁺
^{213}Ra	0	164(3)	1/2 ⁻
^{213m}Ra	1770(7)	$2.15(7) \cdot 10^{-3}$	(17/2 ^{+/−})

with 96.9% enrichment of the isotope ^{170}Er ($326\text{ }\mu\text{g}/\text{cm}^2$) was used to produce ^{213}Ra . In the second experiment in April 2010, the same target was irradiated with a ^{40}Ar beam at an energy of 4.7 MeV/u for the formation of $^{203-205}\text{Rn}$. In the third experiment in October 2011, a beam of ^{50}Ti of 4.55 MeV/u was shot on a gadolinium target with 97.8% enrichment of the isotope ^{160}Gd ($393\text{ }\mu\text{g}/\text{cm}^2$), for the production of $^{204-206}\text{Rn}$. The corresponding reaction cross sections calculated with

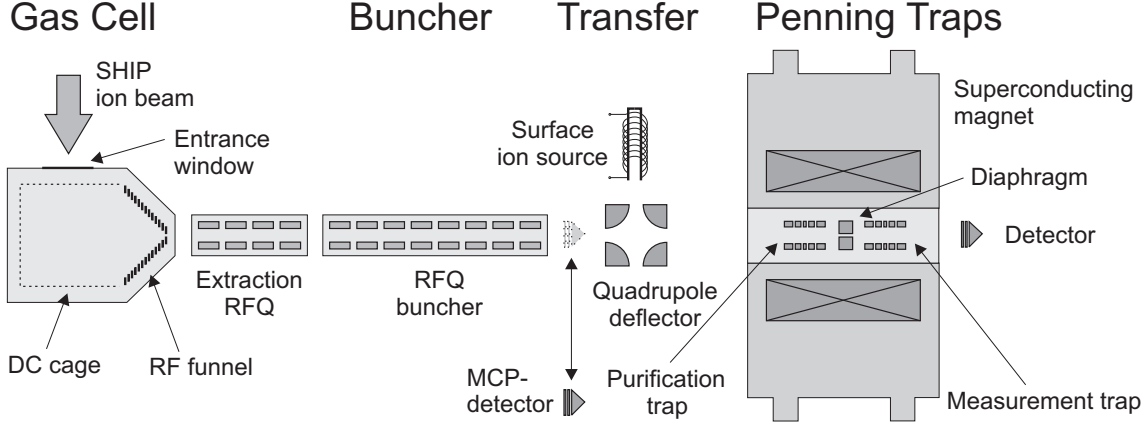


Fig. 2: Experimental setup of the SHIPTRAP apparatus [9]. For details see text.

the statistical-model code HIVAP (Heavy Ion eVAP-oration) [13] are listed in Table 2.

Table 2: Production cross sections calculated with HIVAP [13] for the nuclides investigated and the reactions used for the present measurements. The cross sections given for ^{nat}Dy are the sum of the cross sections for all Dy isotopes multiplied with their relative abundance in the target. The values in brackets of reactions that have not been used are included for comparison. The calculated reaction cross sections are accurate within a factor of three.

Nuclide	Reaction cross sections in mbarn		
	$^{48}\text{Ca} + ^{nat}\text{Dy}$	$^{40}\text{Ar} + ^{170}\text{Er}$	$^{50}\text{Ti} + ^{160}\text{Gd}$
^{203}Rn	(0.01)	0.0002	(0.000008)
^{204}Rn	1.0	2.3	2.3
^{205}Rn	3.3	6.5	12.2
^{206}Rn	5.5	(0.6)	1.8
^{207}Rn	5.5	(0.004)	(0.02)
	$^{48}\text{Ca} + ^{170}\text{Er}$		
^{213}Ra	10		

The evaporation residues were separated from the projectiles by the velocity filter SHIP [10]. Mainly radon isotopes, but also astatine and polonium (with a 10% and 5% production rate of all radon isotopes, respectively), entered the gas cell [14] through a titanium window of $3.6\,\mu\text{m}$ thickness. The ions were slowed down and thermalized in high-purity helium buffer gas at a pressure of 60 mbar. After passing a Radio-Frequency-Quadrupole (RFQ) structure, *i.e.* the extraction RFQ, the ions were further

cooled and accumulated in an RFQ buncher.

To estimate the charge-state distribution of radon and radium ions, the RF amplitudes of the extraction RFQ and the RFQ buncher were set such that one charge state at a time was able to pass both devices [15]. The number of transmitted ions was counted with a micro-channel plate detector behind the

buncher (see Fig. 2). The ratio between singly and doubly charged ions was 1.3 for the radon isotopes and 0.3 for radium, respectively. Thus, settings optimized for singly charged radon and doubly charged radium ions were used.

The ion bunches were injected into the tandem Penning-trap system placed in a 7-T superconducting magnet. There, the charged particles were confined in a homogeneous magnetic field and a quadrupolar electrostatic field. In the first (purification) trap an isobarically pure sample of ions was prepared by mass-selective buffer-gas cooling [16]. After passing a pumping barrier [17] of 1.5 mm in diameter and a length of 47 mm, the ions entered the second trap where high-precision mass measurements were performed by use of the Time-of-Flight Ion-Cyclotron-Resonance (ToF-ICR) technique [18]. The mass determination is based on the measurement of the cyclotron frequency

$$\nu_c = \frac{1}{2\pi} \frac{q}{m} B, \quad (1)$$

where q/m is the charge-to-mass ratio of the stored ion. The magnetic-field strength B was determined by measuring the cyclotron frequency of a reference ion with well-known mass. With increasing cyclotron-excitation time T_{exc} the resolving power

R increases according to the Fourier transform of the rectangular excitation function [19] as

$$R \approx \nu_c T_{exc}. \quad (2)$$

The masses of the ions $^{203-207}\text{Rn}^+$ and $^{213}\text{Ra}^{2+}$ were measured with excitation times T_{exc} between 0.6 s and 6 s. As an example, a time-of-flight resonance of $^{206}\text{Rn}^+$ is displayed in Fig. 3. From a fit of the

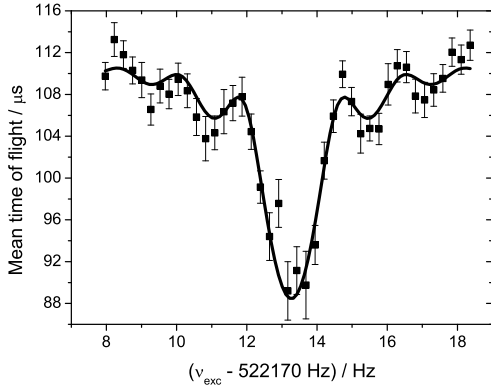


Fig. 3: Time-of-flight ion-cyclotron-resonance of 500 $^{206}\text{Rn}^+$ ions with a cyclotron excitation time $T_{exc} = 0.6$ s. The solid line is a fit of the expected line shape to the data points [20].

resonance function [20] to the data the cyclotron frequency ν_c is obtained with a statistical uncertainty $\delta\nu_c$. A count-rate class analysis [21] was performed and the cyclotron frequency was extrapolated to one detected ion per cycle, including the detector efficiencies, to minimize systematic cyclotron-frequency shifts due to contaminant ions and ion-ion interaction [19, 22].

The magnetic-field strength at the time of the measurement of the ion of interest was interpolated linearly from reference-ion cyclotron-frequency measurements before and after that of the ion of interest. Singly charged $^{133}\text{Cs}^+$ and $^{208}\text{Pb}^+$ ions with the masses $m(^{133}\text{Cs}) = 132.905451933(24)\text{u}$ and $m(^{208}\text{Pb}) = 207.9766521(13)\text{u}$ [23] were used as reference ions. The non-linear magnetic-field fluctuations were considered by including a systematic uncertainty term. For the analysis of the data for the 2009 experiment, a magnetic-field related uncertainty of $\delta_B = 1.3 \cdot 10^{-9}/\text{h}$ [9] was used. In the second and third experiment, magnetic-field fluc-

tuations of the superconducting magnet were reduced by an active stabilization of the bore temperature and the pressure in the LHe cryostat of the solenoid. This resulted in a lower magnetic-field-related uncertainty of $\delta_B = 7.6 \cdot 10^{-11}/\text{h}$ [24]. The mass-dependent uncertainty δ_m [25] was negligible compared to the statistical uncertainty of the present measurements.

From the cyclotron frequency of the ion of interest ν_c and the cyclotron frequency of a reference ion interpolated to the time of the measurement of the ion of interest $\nu_{c,ref}$ results the frequency ratio r_i

$$r_i = \frac{\nu_{c,ref}}{\nu_c} \quad (3)$$

for each measurement i . The atomic mass m of the nuclide is then determined for ions of charge state z via

$$m = r \frac{z}{z_{ref}} (m_{ref} - z_{ref} m_e) + z m_e, \quad (4)$$

where r is the weighted average frequency ratio, m_e is the electron mass and m_{ref} and z_{ref} are the atomic mass and the charge state, respectively, of the reference ion.

The statistical uncertainty δr_i for the individual frequency ratio r_i is given by

$$\delta r_{i,stat} = r_i \sqrt{(\delta\nu_{c,ref}/\nu_{c,ref})^2 + (\delta\nu_c/\nu_c)^2}. \quad (5)$$

Furthermore, the magnetic-field related uncertainty δ_B is added quadratically,

$$\delta r_i = \sqrt{\delta r_{i,stat}^2 + (\delta_B \cdot \Delta t \cdot r_i)^2}, \quad (6)$$

where Δt is the time between two consecutive reference measurements. The duration between two consecutive measurements is a few hours depending on the production rate of the ion of interest. The internal uncertainty of the average frequency ratio r is given by

$$\delta r_{int} = \sqrt{\frac{1}{\sum_i^N 1/\delta r_i^2}}. \quad (7)$$

The external uncertainty

$$\delta r_{ext} = \sqrt{\frac{\sum_i^N 1/\delta r_i^2 \cdot (r_i - r)^2}{(N-1) \cdot \sum_i^N 1/\delta r_i^2}} \quad (8)$$

Table 3: Results of the mass measurements of the isotopes $^{203-207}\text{Rn}(Z=86)$ and $^{213}\text{Ra}(Z=88)$. The columns from left to right display the nuclide, the reference ion, the number of the experiment N_{run} and the number of resonances taken in this run N_{res} . N_{ion} is the number of ions that have been collected for the ion of interest and T_{exc} is the applied excitation time. The last two columns show the measured frequency ratio r that includes the systematic uncertainties^a, and the corresponding atomic mass excess ME_{exp} .

nuclide	reference	N_{run}	N_{res}	N_{ion}	$T_{\text{exc}} / \text{s}$	r	$ME_{\text{exp}} / \text{keV}$
$^{203\text{m}}\text{Rn}^+$	$^{208}\text{Pb}^+$	2	3	6281	2,4,6	0.976041188(144)	-5783(28)
$^{204}\text{Rn}^+$	$^{133}\text{Cs}^+$	1	1	261	0.6	1.534862924(448)	-8050(55)
$^{204}\text{Rn}^+$	$^{208}\text{Pb}^+$	2	1	1143	4	0.9808381913(452)	-7961(9)
$^{204}\text{Rn}^+$	$^{208}\text{Pb}^+$	3	3	609	1	0.980837927(119)	-8012(23)
$^{205}\text{Rn}^+$	$^{133}\text{Cs}^+$	1	10	7075	0.6,1	1.542390116(379)	-7677(47)
$^{205}\text{Rn}^+$	$^{208}\text{Pb}^+$	2	3	8560	1,2,4	0.9856477478(526)	-7707(10)
$^{205}\text{Rn}^+$	$^{208}\text{Pb}^+$	3	3	4873	1	0.9856478631(975)	-7684(19)
$^{205}\text{Rn}^+$	$^{133}\text{Cs}^+$	3	1	2957	1	1.542390124(215)	-7676(27)
$^{206}\text{Rn}^+$	$^{133}\text{Cs}^+$	1	6	3309	0.6	1.549902464(113)	-9141(14)
$^{206}\text{Rn}^+$	$^{208}\text{Pb}^+$	3	3	2993	1	0.9904486157(726)	-9136(14)
$^{207}\text{Rn}^+$	$^{133}\text{Cs}^+$	1	9	4820	0.6	1.557430335(210)	-8685(26)
$^{213}\text{Ra}^{2+}$	$^{133}\text{Cs}^+$	1	3	1397	0.6	0.8013220900(456)	342(11)

^a The uncertainties of the frequency ratios are given with three digits to avoid any accumulation of rounding errors that may enter the Atomic-Mass Evaluation [23].

considers the scattering of the single frequency ratios. The larger of these two values was taken as the uncertainty δr . Finally, a relative systematic uncertainty $\delta r_{\text{sys}} = 4.5 \cdot 10^{-8}$ [25] was added quadratically. The final uncertainty δr_{total} is thus given by

$$\delta r_{\text{total}} = \sqrt{\delta r^2 + (r \cdot \delta r_{\text{sys}})^2}. \quad (9)$$

3 Results and discussion

3.1 Frequency ratios and mass excess values

The frequency ratios obtained in the three experiments are listed in Table 3. The relative mass uncertainty was on average $7 \cdot 10^{-8}$. Instead of the masses m themselves, often the mass excess values

$$ME = m - A \cdot u \quad (10)$$

are given [23], where A is the atomic mass number and the atomic mass unit

$u = 931.494013(37)\text{MeV}/c^2$ [26]. The resulting mass-excess values of the nuclides investigated as derived from the frequency ratios (Table 3) are listed in Table 4. For nuclides whose mass has been determined with different reference ions the weighted average for the mass excess is given. The

results are compared to the values of the Atomic-Mass Evaluation 2003 [23] in Fig. 4. The mass uncertainties of the isotopes ^{205}Rn , ^{206}Rn and ^{213}Ra were reduced. In the following, the nuclides are discussed in detail.

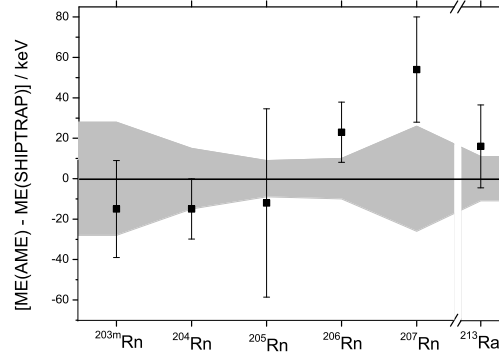


Fig. 4: Differences between the AME values $ME(\text{AME})$ (black points) and the measured mass-excess values $ME(\text{SHIPTRAP})$. The grey band indicates the uncertainties of the present results. For a detailed discussion see text.

Table 4: Comparison between the mass-excess values of the AME (ME_{AME} [23]) and the present experimental results (ME_{exp}). The difference $\Delta = ME_{AME} - ME_{exp}$ between the AME values and the experimental results is shown in the fourth column.

Nuclide	ME_{AME} / keV	ME_{exp} / keV	Δ / keV
^{203m}Rn	-5798(24)	-5783(28)	-15(36)
^{204}Rn	-7984(15)	-7969(15)	-15(21)
^{205}Rn	-7710(50)	-7698(9)	-12(51)
^{206}Rn	-9116(15)	-9139(10)	23(18)
^{207}Rn	-8631(26)	-8685(26)	54(37)
^{213}Ra	358(20)	342(11)	16(23)

^{203}Rn

In addition to the ground state of ^{203}Rn with a half-life of 44(2) s, there is an isomeric state with a half-life of 26.9(5) s. From decay spectroscopy [11] the excitation energy is known to be 362(5) keV. This long-lived excited state has been tentatively assigned a spin and parity of $13/2^+$ [11], while the ground state is tentatively assigned a spin and parity of $3/2^-$ (a spin and parity of $5/2^-$ cannot be unambiguously excluded). Based on their half-lives, both states could have been present in our measurement. The measurements with a resolving power from $1 \cdot 10^6$ to $3 \cdot 10^6$, corresponding to excitation times T_{exc} from 2 s to 6 s, were suitable to resolve states with excitation energy differences higher than 150 keV. A frequency range of 2 Hz that covers an energy interval of approximately 750 keV was scanned. However, only one resonance was found.

The measured mass excess of the isotope ^{203}Rn of $ME = -5783(28) \text{ keV}$ deviates from the AME value for the ground-state mass of $-6160(24) \text{ keV}$ by $-377(36) \text{ keV}$ but agrees well with the ME of the isomeric state of $-5798(24) \text{ keV}$. Thus, we assume that in this particular fusion-evaporation reaction the high-spin state was much stronger populated than the ground-state. The AME mass value was determined via alpha-gamma-spectroscopy [27, 28, 29, 30]. The decay chain is fixed by a direct mass measurement of the daughter nuclide ^{199}Po in the experimental storage ring ESR at GSI [8].

^{204}Rn

The mass of this isotope was determined in all three runs (see Table 3). In the performed experiments the mass-excess values $-8050(55) \text{ keV}$, $-7961(9) \text{ keV}$ and $-8012(23) \text{ keV}$ were obtained. A large scattering between the experimental results is observed. The final result is mainly determined by the frequency ratio recorded in the second experiment with an excitation time of 4 s, a considerably higher statistics than the other resonances and practically no background. The resulting average mass-excess value of $-7969(15) \text{ keV}$ confirms the AME value of $-7984(15) \text{ keV}$ based on alpha-gamma spectroscopy of ^{204}Rn [27, 28, 29] and the directly measured mass of the daughter nuclide ^{200}Po in the ESR [8].

^{205}Rn

The mass of ^{205}Rn was also measured in all three runs. The mass-excess values determined in all three experiments are in good agreement with each other. The mass excess was determined as $-7698(9) \text{ keV}$. This result is in good agreement with the AME value $-7710(50) \text{ keV}$ [23]. The latter was derived from alpha-decay spectroscopy [27, 28, 31] and direct mass measurements of the daughter nuclide ^{201}Po in the ESR [8]. The ground state has a half-life of 170(4) s and a spin and parity assigned as $5/2^-$ [11]. According to recent investigations [12], this isotope has an isomeric state with spin and parity of $13/2^+$ at an excitation energy of 657.1(5) keV with an estimated half-life of more than 10 s. The excitation energy of the long-lived state was determined via gamma-conversion-electron coincidence measurements. However, due to contaminations in the concerning gamma line this assignment is tentative. With typical cyclotron excitation times of 1 s the mass resolution of the Penning trap is about 400 keV, which is sufficient to detect the presence of this isomer. The scanned frequency range of 5 Hz covers an energy interval of approximately $\pm 900 \text{ keV}$. However, no admixture of the isomer to the ground state was detected.

The discrepancy between the presence of the isomeric state in ^{203}Rn and the ground-state in ^{205}Rn could link to an overestimation of the half-life of ^{205m}Rn in [12]. An isomeric state with a half-life in the range of milliseconds, and shorter, would have been completely decayed when the measurement cycle is finished, and thus only the ground-

state would remain. Due to the unclear results in [12], an unambiguous correlation between the $13/2^+$ state and the excitation energy of 657.1(5) keV cannot be made. An isomeric state with an excitation energy higher than 900 keV would not have been observed in the present measurement.

^{206}Rn

The measured mass excess of ^{206}Rn is -9139(10) keV. The mass-excess values of the first and the third experiments are in good agreement with each other. The difference between the mass-excess values given in the AME and the SHIPTRAP result is 23(18) keV. The AME value is based on alpha-decay chains [27, 28, 32] linked to a direct mass measurement of ^{202}Po [8].

^{207}Rn

The isotope ^{207}Rn has an isomeric state at an excitation energy of 899.1(10) keV and a spin and parity of $13/2^+$ [11]. With a half-life of 184.5(9) μs this isomer has decayed before it reaches the measurement trap. Thus, we can conclude that only the ground state with a spin and parity of $5/2^-$ has been investigated. The measured mass excess of -8685(26) keV deviates by 54(37) keV from the AME data. The AME input values [27, 32, 33] have been determined via alpha-gamma spectroscopy and direct mass measurement of the daughter nuclide ^{203}Po in the ESR [8].

^{213}Ra

The isomeric state of this isotope (with a tentative spin-parity assignment of $17/2^+$ or $17/2^-$) has an excitation energy of 1770(7) keV and a half-life of 2.15(5) ms. The cycle time of the whole measurement is orders of magnitude longer. Thus, only the ground state was detected. The difference between the mass excess determined in this work (342(11) keV) and the AME value (358(20) keV) is 16(23) keV. The AME mass value of ^{213}Ra is based on alpha-decay chains [34, 35] to ^{205}Po , whose mass has been measured directly in the ESR [8].

3.2 Two-Neutron Separation Energies

The two-neutron separation energy

$$S_{2n}(Z, N) = [2m_N + m(Z, N-2) - m(Z, N)] \cdot c^2, \quad (11)$$

where m_N is the neutron mass, is an often-used quantity to probe the evolution of the nuclear structure. The S_{2n} values show a smooth decrease as the neu-

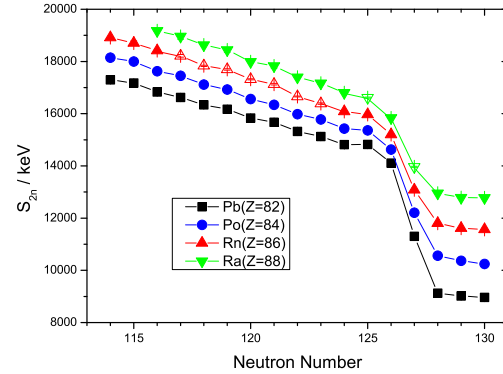


Fig. 5: (color online) The two-neutron separation energies S_{2n} as a function of the neutron number N for Pb (black squares), Po (blue circles), Rn (red triangles) and Ra isotopes (green triangles). The open symbols indicate the S_{2n} determined from the experimental results of this work. Mass values from the AME 2003 were used for the calculation of the S_{2n} values if only one experimental result was available. For Ra the masses of isotopes with $N < 114$ are not known.

tron shell is filled, here between the magic numbers $N = 82$ and $N = 126$ (see Fig. 5). At a shell closure there is a steep decrease in the S_{2n} values due to the reduced binding for the first neutron above the magic neutron number. The S_{2n} values derived from the experimental results between $N = 114$ and $N = 126$ including our work for the neutron-deficient Rn isotopes follow this trend nicely. This indicates that the deformation of the radon nuclei with four additional protons compared to Pb, with the magic proton number $Z = 82$, is comparable to those of the Pb isotopes [36], which confirms the results of previous investigations [37]. The new experimental two-neutron separation energies were compared to the values obtained from

the liquid-drop model [38] with the coefficients of the semi-empirical mass formula taken from [39] in the range between $N = 114$ and $N = 125$ (see Fig. 6).

The liquid-drop model treats a nucleus as a drop

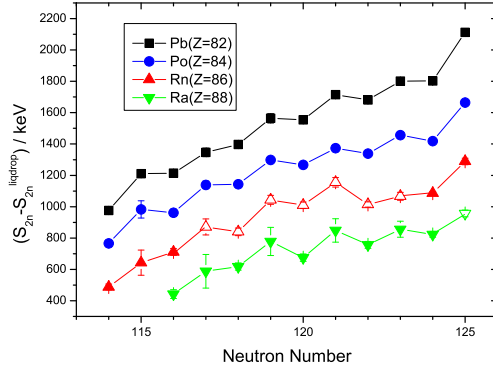


Fig. 6: (color online) Difference of the two-neutron separation energies determined from the Atomic-Mass Evaluation and this work and the two-neutron separation energies calculated with the liquid-drop model for Pb, Po, Rn and Ra isotopes between $N = 114$ and $N = 125$. The S_{2n} values determined from the results of this work are indicated by open symbols. Mass values from the AME 2003 were used for the calculation of the S_{2n} values if only one experimental result was available. For details see text.

of an incompressible fluid. From the difference of the two-neutron separation energies and theoretical predictions of the liquid-drop model for close-to-spherical nuclei one can obtain the size of the shell effects. In Fig. 6 the energy difference between the liquid-drop model and experimental results decrease as we move away from the closed proton shell configuration of Pb and from the closed $N = 126$ neutron shell. This is linked to the incapability of the liquid-drop model to describe shell effects. Moreover, an odd-even staggering superimposed to the linear increase is observed which becomes more and more emphasized for nuclides with higher proton numbers. The pairing term of the liquid drop model has a negligible effect on the calculated two-neutron separation energies and is therefore insufficient to describe the odd-even staggering observed in Fig. 6. A more elaborated model to describe the pairing is needed to explain the ob-

served behaviour of the two-neutron separation energies.

4 Summary

Precision mass measurements of $^{203-207}\text{Rn}$ and ^{213}Ra were performed with the Penning-trap mass spectrometer SHIPTRAP. Overall, the AME values [23] based on nuclear decays agree with these first results of direct mass measurements. The uncertainties in the mass-excess values of the isotopes ^{205}Rn , ^{206}Rn and ^{213}Ra were reduced to about 10 keV. Furthermore, in the region of $N = 116$ to 122, there are indications for a proton-number dependent odd-even staggering in excess of the description by the liquid-drop model.

Acknowledgments

We acknowledge the support of the German BMBF under Grant 06GF186I, 06GF9103I, 05P12HGFN5, 06ML9148, under the WTZ Grant RUS-07/015 and the Max-Planck Society. C.D., G.M. and L.S. also thank for support by the GSI F & E program. D. N. and Yu. N. thank the Russian Minobrnauki under grant 2.2.

References

1. M. Brodeur *et al.*, Phys. Rev. Lett. 108 (2012) 052504
2. U. Hager *et al.*, Phys. Rev. C 75 (2007) 064302
3. M. Arnould, S. Goriely and K. Takahashi, Phys. Rep. 450 (2007) 97
4. M. Dworschak *et al.*, Phys. Rev. C 81 (2010) 064312
5. M. Block *et al.*, Nature 463 (2010) 785
6. K. Blaum, Phys. Rep. 425 (2006) 1
7. L. Schweikhard and G. Bollen (eds.), special issue of Int. J. Mass Spectrom. 251 (2006)
8. Yu. A. Litvinov *et al.*, Nucl. Phys. A 756 (2005) 3
9. M. Block *et al.*, Eur. Phys. J. D 45 (2007) 39
10. S. Hofmann and G. Münzenberg, Rev. Mod. Phys. 72 (2000) 733
11. Evaluated Nuclear Structure Data File (ENSDF), www.nndc.bnl.gov/ensdf/
12. A.Y. Deo *et al.*, Phys. Rev. C 81 (2010) 024322
13. W. Reisdorf, Z. Phys. A 300 (1981) 227

14. J. B. Neumayr *et al.*, Nucl. Instrum. Methods Phys. Res., Sect. B 244 (2006) 489
15. W. Paul, Rev. Mod. Phys. 62 (1990) 531
16. G. Savard *et al.*, Phys. Lett. A 158 (1991) 247
17. D. Neidherr *et al.*, Nucl. Instrum. Methods Phys. Res., Sect. B 266 (2008) 4556
18. G. Gräff, H. Kalinowsky and J. Traut, Z. Phys. A 297 (1980) 35
19. G. Bollen *et al.*, J. Appl. Phys. 68 (1990) 4355
20. M. König *et al.*, Int. J. Mass Spectrom. Ion Processes 142 (1995) 95
21. A. Kellerbauer *et al.*, Eur. Phys. J. D 22 (2003) 53
22. L. Schweikhard *et al.*, Eur. J. Mass Spectrom. 11 (2005) 457
23. G. Audi, A. H. Wapstra and C. Thibault, Nucl. Phys. A 729 (2003) 337
24. C. Droese *et al.*, Nucl. Instrum. Methods Phys. Res., Sect. A 632 (2011) 157
25. A. Chaudhuri *et al.*, Eur. Phys. J. D 45 (2007) 47
26. P. J. Mohr and B. N. Taylor, J. Phys. Chem. Ref. Data 28 (1999) 1713
27. J. Wauters *et al.*, Phys. Rev. C 47 (1993) 1447
28. K. Valli, M. J. Nurmi and E. K. Hyde, Phys. Rev. 159 (1967) 1013
29. M. J. LeDdy *et al.*, Phys. Rev. C 51 (1995) 1047(R)
30. M. Leino *et al.*, Z. Phys. A 355 (1996) 157
31. P. Hornshøj *et al.*, Nucl. Phys. A 163 (1971) 277
32. N. A. Golokov *et al.*, Izvestiya Akademii Nauk SSSR seriya Fizicheskaya 35 (1971) 2272
33. K. Valli, E. K. Hyde and W. Treytl, J. Inorg. Nucl. Chem. 29 (1967) 2503
34. K. Valli, W. Treytl and E. K. Hyde, Phys. Rev. 161 (1967) 1284
35. D. G. Raich *et al.*, Z. Phys. A 279 (1976) 301
36. R.C. Thompson *et al.*, J. Phys. G 9 (1983) 443
37. J. Kilgallon *et al.*, Phys. Lett. B 405 (1997) 31
38. C. F. v. Weizsäcker, Z. Phys. 96 (1935) 431
39. J. W. Rohlfs, *Modern Physics from α to $Z=0$* (1994) Wiley